JSR Publications

Available Online

J. Sci. Res. **15** (2), 489-508 (2023)

JOURNAL OF SCIENTIFIC RESEARCH

www.banglajol.info/index.php/JSR

Theoretical Explorations of Structural, Electronic, and Spectroscopic Properties of a Series of Ruthenium Schiff-Base Complexes

C. G. Sarkar*

Department of Chemistry, Hooghly Mohsin College, Chinsurah, Hooghly, Pin-712101, West Bengal, India

Received 31 August 2022, accepted in final revised form 5 November 2022

Abstract

The present work concentrates on theoretical investigations of the substituent effects on the reactivity, electronic properties, and UV-vis spectra of a series of ruthenium-Schiff base complexes using density functional theory (DFT). Four complexes are studied herein, where *N*-(2′-hydroxyphenyl)benzaldimine is the Schiff base differing in the *para*-substituent (R) on the benzaldehyde fragment (R = CH_3, H, Cl, CF_3). B3LYP/SDD-6-31G(d,p) level of theory has been used for computational studies (Gaussian 16). All the structures have been optimized, and the compositions of the frontier molecular orbitals have been analyzed. The energies of HOMO and LUMO and the global indices parameters have been calculated, which reveals that $[Ru(PPh_3)_2(CO)(L\text{-}CF_3)]$ is the most reactive complex and $[Ru(PPh_3)_2(CO)(L\text{-}Cl)]$ the least. Time-dependent density functional theory (TDDFT) has been performed to study the electronic absorption parameters. The effect of solvent polarity upon absorption spectra has also been observed. It is found that the lowest energy absorptions in all the complexes show a blue shift with the increase in polarity of the solvent. Natural bond orbital (NBO) analysis of the complexes has been conducted to examine the charge distribution on the donor and the acceptor atoms along with their variation with change in the *para*-substituent.

Keywords: DFT and TDDFT studies; Global indices; NBO analysis; Ruthenium complexes.

© 2023 JSR Publications. ISSN: 2070-0237 (Print); 2070-0245 (Online). All rights reserved.
doi: http://dx.doi.org/10.3329/jsr.v15i2.61478 J. Sci. Res. **15** (2), 489-508 (2023)

1. Introduction

Schiff bases are a class of ligands with an azomethine group (C=N) classically synthesized by condensing a carbonyl group and a primary amine [1]. They are distinguished in their ability to coordinate with metal centers having variable oxidation states through two or more electron-donating sites [2-26]. The coordination chemistry of Schiff bases has always been an active area of research because the metal complexes of this ligand have possessed a wide variety of interesting biological properties [2,3,5-7,9,10,12,13,15,16,18,21,25]. The complexes also exhibited important catalytic

* *Corresponding author*: chhandasi22@gmail.com

[12,18,20], thermal [7,9-12,14-16,20,22-26], and electrochemical characteristics [4,8,17]. These traits of the complexes are highly dependent on the coordination sphere around the central metal ion and thus modifying the substituents of the bonded Schiff bases has produced numerous complexes with fascinating properties. Herein a series of ruthenium complexes are selected [27] with *N*-(2′-hydroxyphenyl)benzaldimine (**1**) as the chief coordinating ligand. The ligand (**1**), along with its coordination modes in the complexes (**2**), are shown in Fig. 1. It is worth mentioning at this point that the chemistry of ruthenium complexes is extremely important because of their captivating electrochemical, catalytic, photophysical and photochemical and biological activities [28-37]. The syntheses, spectral and cyclic voltammetric properties of three complexes of the series where R= CH_3, H, Cl, have been discussed in the literature [27]. Structural parameters, as determined by X-ray crystallography of one of the complexes in the series, have been reported [27]. However, as far as our literature survey has revealed, no systematic theoretical investigations of the series of complexes have been performed. Keeping this in mind, the present study aims to impart a density functional theory (DFT) and time-dependent density functional theory (TDDFT) study to explain the complexes' electronic, structural, and spectral properties. Today, DFT is one of the primary tools to interpret and predict a wide range of physical, chemical, and biological properties of coordination complexes [38-44]. It has also found application in elucidating the reactivity of molecules [45], reaction pathways [46], and catalysis [47,48]. The DFT method has also been widely applied for theoretical studies of many Schiff base complexes [2,3,5-7,15,24,25]. The present article considers the following aspects of the ruthenium complexes of *N*-(2′-hydroxyphenyl)benzaldimines: geometry optimization, IR and UV-vis spectral properties, electronic properties, compositions and energies of their frontier molecular orbitals.

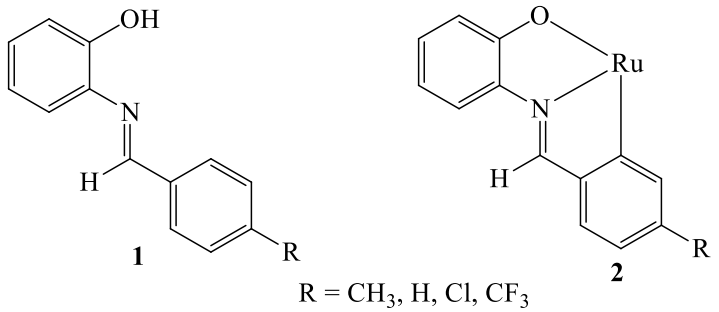

Fig. 1. N-(2′-hydroxyphenyl)benzaldimine (**1**) and its coordination mode in the complexes (**2**).

2. Computational Methods

Geometry optimizations of the complexes were performed using density functional theory (DFT), and spectral absorption analyses were carried out with the help of time-dependent density functional theory (TDDFT) in Gaussian 16 [49]. In all the calculations Gaussian 16 [B3LYP/SDD-6-31G(d,p)] package, with the help of the GaussView visualization

program, was used. The representation of the optimized structures of the complexes was accomplished using Avogadro. The ONIOM method was utilized, and the complexes were optimized via a two-level approach. This approach was undertaken to find the effective balance between the computational costs and the accuracy of the data obtained [50]. The chemically significant part of the complexes was treated with DFT, while the rest of the molecules were tackled by the semi-empirical method. The phenyl groups of the coordinated triphenylphosphines (PPh_3) were considered as the lower level using the PM6 level of theory, while the remaining atoms (higher level) were handled within the B3LYP framework. Within the high-level treatment, a 6-31G(d,p) basis set was applied for the C, H, O, N, P, Cl, and F atoms. It is a split-valence double-zeta basis set along with polarization functions that appropriately describe the core, valence orbitals, and chemical bonds. The ruthenium atoms were assigned the SDD basis set. The SDD basis set fuses the DZ with the Stuttgart-Dresden effective core potential (ecp) [51]. This helped in overcoming the description of relativistic effects in core electrons by treating only valence electrons and reducing the computational cost. The use of an SDD basis set for ruthenium atoms is well prevalent in the literature [52-54]. The vibrational frequency was evaluated so that the optimized geometry corresponded to local minima, and there were only positive eigenvalues. Natural bond orbital (NBO) analysis was done using the NBO of Gaussian 16. The frontier molecular orbital analysis and TDDFT studies were carried out by replacement of the phenyl rings of the triphenylphosphines with methyl groups to simplify the calculations [55]. TDDFT studies were conducted in vacuum as well as in three different solvents, *viz*. dichloromethane (DCM), ethanol and dimethylsulphoxide (DMSO). GaussSum was used to calculate the percentage contributions of different molecular fragments to each molecular orbital. The global indices, *viz*., chemical potential (μ), chemical hardness (η), and electrophilicity index (ω) were calculated considering molecules in the gas phase, as follows [56,57]:

$$\mu \approx (E_{HOMO}+E_{LUMO})/2 \quad (1)$$

$$\eta \approx E_{LUMO}-E_{HOMO} \quad (2)$$

$$\omega = \mu^2/2\eta \quad (3)$$

3. Results and Discussion

As delineated in the introduction, the principal objective of the present work is to investigate the structural and electronic parameters and spectroscopic properties of a series of ruthenium Schiff base complexes with the help of density functional theory. Four *N*-(2'-hydroxyphenyl)benzaldimines (**1**), differing in the inductive effect of the *para*-substituents (R, R=CH_3, H, Cl, CF_3) on the benzaldehyde group, have been utilized for the computational studies to understand their effects, if any, on the properties of the complexes. These ligands are abbreviated as H_2L-R, where H_2 signifies two protons, the phenolic proton and one *ortho* proton of the phenyl ring in the benzaldehyde moiety, which undergoes dissociation upon formation of the complexes, and R represents the *para*-substituent. The complexes are depicted as [Ru(PPh_3)$_2$(CO)(L-R)].

3.1. *Structural properties*

Four complexes *viz*. $[Ru(PPh_3)_2(CO)(L\text{-}CH_3)]$, $[Ru(PPh_3)_2(CO)(L\text{-}H)]$, $[Ru(PPh_3)_2(CO)(L\text{-}Cl)]$ and $[Ru(PPh_3)_2(CO)(L\text{-}CF_3)]$ were optimized using ONIOM method as stated earlier. The bond parameters of $[Ru(PPh_3)_2(CO)(L\text{-}H)]$ as obtained from X-ray crystallography [27] are compared with the optimized values in Table 1. The optimized ground state geometries of all the complexes are shown in Fig. 2. The optimized structures of the free ligands *viz*., $H_2L\text{-}CH_3$, $H_2L\text{-}H$, $H_2L\text{-}Cl$, and $H_2L\text{-}CF_3$ are presented in Fig. S1 (Supporting Information). The relevant geometrical parameters of the three other complexes are given in Table S1 (Supporting Information). Since no experimental values of bond lengths and bond angles are available for these complexes to the best of our knowledge, the comparison between the experimental and calculated data was not possible for them. For the $[Ru(PPh_3)_2(CO)(L\text{-}H)]$ complex, it is found that the optimized structural parameters are in quite good agreement with the experimental values. In the case of bond lengths, the maximum difference is 0.124Å (Ru1-N2), and for bond angles, the maximum discrepancy is 9.33° for Ru1-C73-O3 angle. These differences are probably due to the non-consideration of lattice interactions in the case of DFT computations because the calculations were accomplished with molecules in the gas phase [58,59]. A comparison of the structural parameters between the four complexes revealed that they are in unison.

Table 1. Bond distances (Å) and bond angles (°) of $[Ru(PPh_3)_2(CO)(L\text{-}H)]$.

Bond distances (Å)			Bond angles (°)		
Bonds	Optimized	Experimental	Angles	Optimized	Experimental
Ru1-P5	2.41971	2.401(2)	P6-Ru1-P5	177.109	177.76(7)
Ru1-P6	2.42701	2.354(3)	C95-Ru1-O4	156.522	154.70(2)
Ru1-O4	2.21055	2.107(6)	C73-Ru1-N2	175.942	172.50(3)
Ru1-N2	2.11598	1.992(5)	Ru1-C73-O3	177.329	168.0(8)
Ru1-C95	2.07167	2.089(8)	C95-Ru1-N2	79.577	77.2(3)
Ru1-C73	1.85033	1.860(6)	N2-Ru1-O4	76.950	77.5(2)

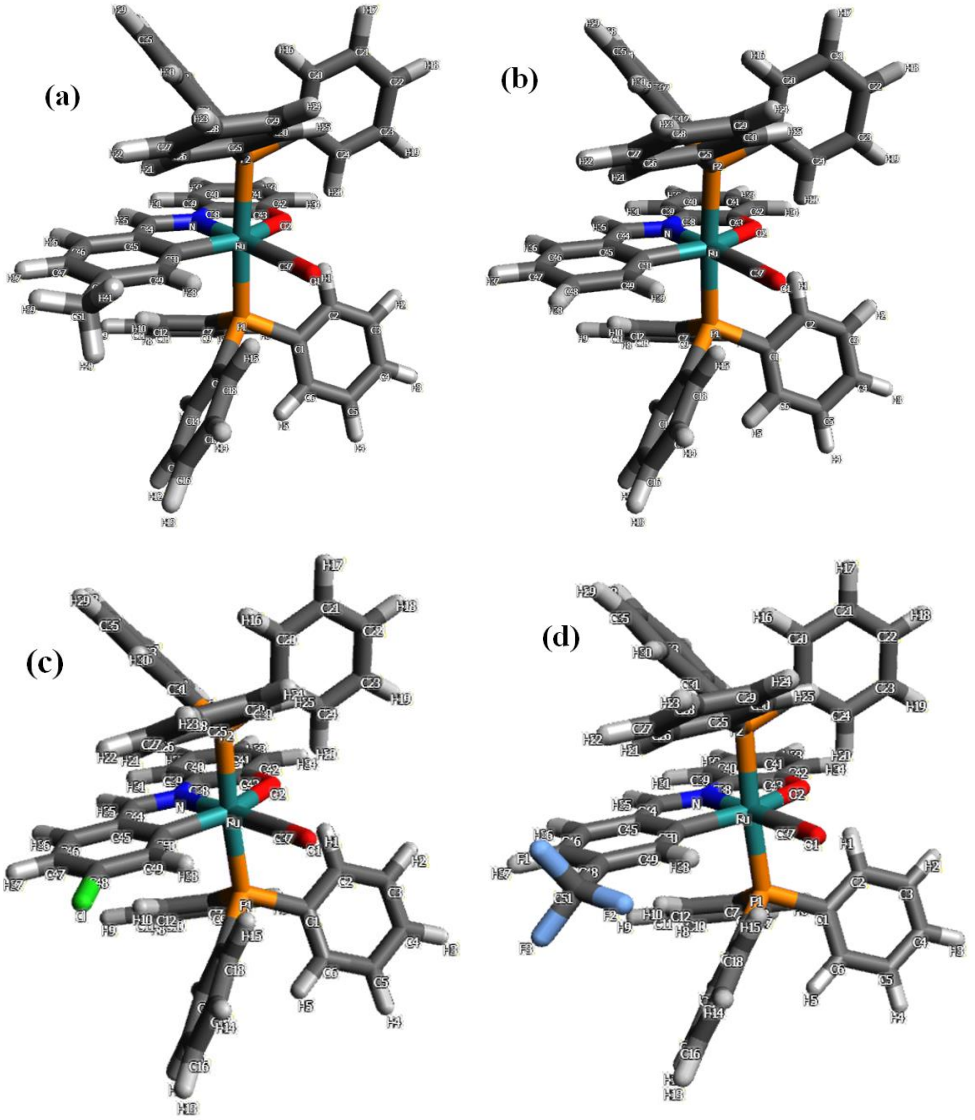

Fig. 2. Optimized structures of a) $[Ru(PPh_3)_2(CO)(L\text{-}CH_3)]$ b) $[Ru(PPh_3)_2(CO)(L\text{-}H)]$ c) $[Ru(PPh_3)_2(CO)(L\text{-}Cl)]$ d) $[Ru(PPh_3)_2(CO)(L\text{-}CF_3)]$.

3.2. *Frontier molecular orbital properties*

The frontier molecular orbitals have important contributions to a coordination complex's different physical and chemical properties. Following Fukui's theory [60,61], the reactivity of the complexes can be predicted by calculating the energy gap (ΔE) between the highest occupied molecular orbital (HOMO) and the lowest unoccupied molecular orbital (LUMO). According to Fukui, when the energy gap between HOMO and LUMO

decreases, the reactivity of the species increases, and vice versa. Fig. 3 shows the contour plots and energies of HOMO and LUMO of the four complexes, along with the difference in energies of HOMO and LUMO [$\Delta E(E_{LUMO}-E_{HOMO})$] in each complex. The global indices, *viz*., chemical potential (μ), chemical hardness (η), and electrophilicity index (ω) of the complexes are listed in Table 2. In the complexes, the phenyl rings of the triphenylphosphines have been replaced by methyl groups to make the calculations less complicated. Such replacements have their instances in literature [55] and it is found that it does not qualitatively alter the parameters of the complexes, and the data obtained can be used to elucidate the properties of corresponding triphenylphosphine complexes. The values reveal that the energies of HOMO and LUMO are increased when an electron-donating substituent is present (CH_3) and vice versa when an electron-withdrawing group (Cl, CF_3) is added. This trend in the change in energy levels of HOMO and LUMO in transition metal complexes, with the addition of electron-withdrawing or donating groups, is well recorded in the literature [62-65].

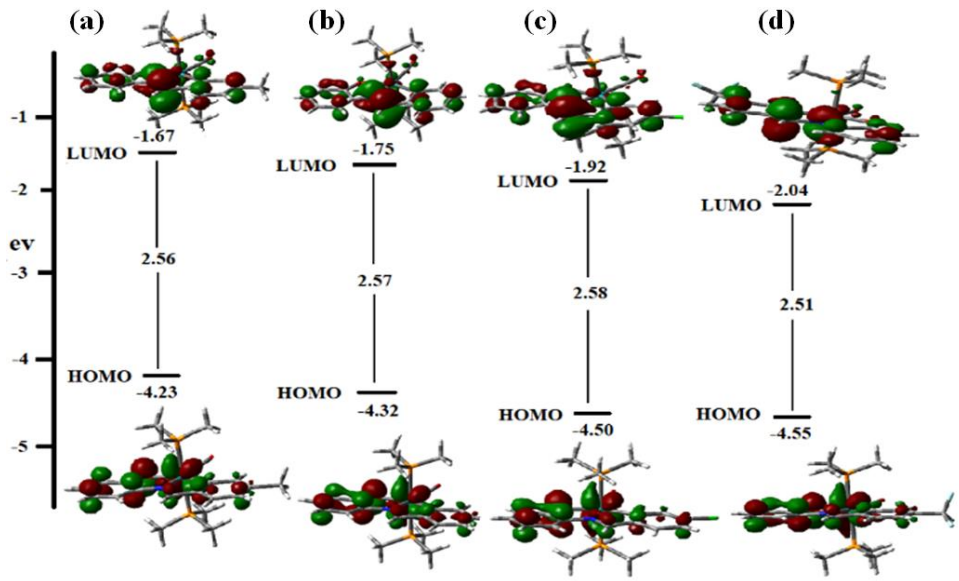

Fig. 3. Contour plots and energies of HOMO and LUMO of a) $[Ru(PPh_3)_2(CO)(L\text{-}CH_3)]$ b) $[Ru(PPh_3)_2(CO)(L\text{-}H)]$ c) $[Ru(PPh_3)_2(CO)(L\text{-}Cl)]$ d) $[Ru(PPh_3)_2(CO)(L\text{-}CF_3)]$.

Table 2. Chemical potentials (μ), chemical hardnesses (η), and electrophilicity indices (ω) of the complexes.

Complexes	μ [eV]	η [eV]	ω [eV]
$[Ru(PPh_3)_2(CO)(L\text{-}CH_3)]$	-2.95	2.56	1.70
$[Ru(PPh_3)_2(CO)(L\text{-}H)]$	-3.04	2.57	1.80
$[Ru(PPh_3)_2(CO)(L\text{-}Cl)]$	-3.21	2.58	2.00
$[Ru(PPh_3)_2(CO)(L\text{-}CF_3)]$	-3.30	2.51	2.17

Although the energies of HOMO and LUMO decrease for both $[Ru(PPh_3)_2(CO)(L\text{-}Cl)]$ and $[Ru(PPh_3)_2(CO)(L\text{-}CF_3)]$, the extent of decrease in energy of LUMO in comparison to that of HOMO is far greater in case of the CF_3 substituted complex. This is because the CF_3 group possesses only a negative inductive effect (-I effect) while the Cl substituent has both a negative inductive effect (-I effect) and positive resonance effect (+R effect). This property of CF_3 and Cl moieties also explains the order of energy gap in the four complexes which reveals that $[Ru(PPh_3)_2(CO)(L\text{-}CF_3)]$ is the most reactive of the complexes and $[Ru(PPh_3)_2(CO)(L\text{-}Cl)]$ the least, although the difference in reactivity is very small. This small difference can be accounted for by the fact that the contribution of the substituent R in the compositions of HOMO and LUMO of the complexes is almost negligible (0-1 %) as expressed in Table 3. Table 3 contains the compositions of HOMO and LUMO of all the complexes. The compositions of other molecular orbitals associated with the electronic transitions in the four complexes are presented in Table S2 (Supporting Information). Thus, the substituent R has very little influence on the reactivity of the complexes. The electrophilicity indices show that $[Ru(PPh_3)_2(CO)(L\text{-}CF_3)]$ is the strongest electrophile and $[Ru(PPh_3)_2(CO)(L\text{-}CH_3)]$ the weakest, as is expected from the inductive effect of the R substituent.

Table 3. Compositions of frontier molecular orbitals of the complexes.

Complexes	Molecular Orbitals	Contribution of Fragments (%)			
		Ru	L-R	PPh_3	CO
$[Ru(PPh_3)_2(CO)(L\text{-}CH_3)]$	LUMO	3	92 (C=N is 66) (CH_3 is 1)	2	3
	HOMO	36	61 (C=N is 26) (CH_3 is 0)	2	1
$[Ru(PPh_3)_2(CO)(L\text{-}H)]$	LUMO	3	93 (C=N is 47)	2	2
	HOMO	34	63 (C=N is 14)	2	1
$[Ru(PPh_3)_2(CO)(L\text{-}Cl)]$	LUMO	3	93 (C=N is 71) (Cl is 1)	2	2
	HOMO	32	65 (C=N is 18) (Cl is 0)	2	1
$[Ru(PPh_3)_2(CO)(L\text{-}CF_3)]$	LUMO	3	93 (C=N is 59) (CF_3 is 1)	2	2
	HOMO	33	64 (C=N is 12) (CF_3 is 0)	2	1

3.3. *Spectral properties*

Infrared spectra of the $[Ru(PPh_3)_2(CO)(L\text{-}CH_3)]$, $[Ru(PPh_3)_2(CO)(L\text{-}H)]$, $[Ru(PPh_3)_2(CO)(L\text{-}Cl)]$ and $[Ru(PPh_3)_2(CO)(L\text{-}CF_3)]$ complexes have been calculated, and they show many bands of varying intensities within 3000–400 cm^{-1}. Designation of each band to a specific vibration has not been attempted. Three strong bands obtained around 486, 680, and 790 cm^{-1} in all the complexes are attributed to the bonded triphenylphosphines. A very intense band at 1870 ($[Ru(PPh_3)_2(CO)(L\text{-}CH_3)]$), 1871 ($[Ru(PPh_3)_2(CO)(L\text{-}H)]$), 2004 ($[Ru(PPh_3)_2(CO)(L\text{-}Cl)]$) and 2006 cm^{-1} ($[Ru(PPh_3)_2(CO)(L\text{-}CF_3)]$) is identified to be due to the coordinated carbonyl group. A moderately intense band observed in the region of 1562-1577 cm^{-1} for the four complexes is assigned to the ν(C=N) of the bonded benzaldimine ligand. All the complexes display

an intense phenolic C-O stretching band between 1347-1352 cm^{-1}. In addition, two weak bands found in the region 500-537 cm^{-1} and 402-433 cm^{-1} are designated to the stretching frequencies of ν(Ru-O) and ν(Ru-N), respectively.

The absorption spectra of the four ruthenium complexes where the phenyl groups of the triphenylphosphines have been replaced by methyl groups [55] have been evaluated using time-dependent density functional theory (TDDFT) in a vacuum and different solvents. Three solvents with increasing polarity are selected, *viz*., dichloromethane (DCM), ethanol, and dimethylsulphoxide (DMSO) to predict their influence, if any, on the absorption properties of the complexes. The calculated absorption parameters are reported in Table 4.

Table 4. Absorption spectral data of the complexes.

Complex	Transition Number	Nature of Transition	CI value	E/eV	Oscillator strength, f	λ_{theo}/ nm	Assignment
$[Ru(PPh_3)_2(CO)(L\text{-}CH_3)]$	1	H→L	0.69752	1.7633	0.0296	703.15	ILCT/MLCT
	2	H-3→L	0.14304	3.2028	0.1034	387.11	ILCT/MLCT
		H-2→L	0.66335				ILCT/MLCT
	3	H-3→L	-0.11154	3.3269	0.0027	372.67	ILCT/MLCT
		H→L+1	0.68611				ILCT/MLCT
	4	H-2→L	0.10101	3.5482	0.0123	349.43	ILCT/MLCT
		H→L+2	0.68998				ILCT/MLCT
$[Ru(PPh_3)_2(CO)(L\text{-}H)]$	1	H→L	0.69785	1.7198	0.0256	720.93	ILCT/MLCT
	2	H-3→L	0.20105	3.1758	0.0962	390.41	ILCT/MLCT
		H-2→L	0.65538				ILCT/MLCT
	3	H-3→L	0.66243	3.2687	0.0128	379.31	ILCT/MLCT
		H-2→L	-0.18222				ILCT/MLCT
	4	H→L+2	0.69143	3.5961	0.0070	344.78	LMCT/MLCT
$[Ru(PPh_3)_2(CO)(L\text{-}Cl)]$	1	H→L	0.69639	1.8007	0.0362	688.53	ILCT/MLCT
	2	H-3→L	-0.19373	3.1864	0.1011	389.11	ILCT/MLCT
		H-2→L	0.65152				ILCT/MLCT
		H→L+2	0.10784				LMCT/ILCT
	3	H-4→L	0.10499	3.3010	0.0075	375.59	ILCT
		H-3→L	0.65312				ILCT/MLCT
		H-2→L	0.16312				ILCT/MLCT
		H→L+2	0.10250				LMCT/ILCT
	4	H-4→L	-0.11757	3.5982	0.0269	344.57	ILCT
		H-2→L	-0.12220				ILCT/MLCT
		H→L+2	0.66371				LMCT/ILCT
$[Ru(PPh_3)_2(CO)(L\text{-}CF_3)]$	1	H→L	0.69683	1.7395	0.0318	712.78	ILCT/MLCT
	2	H-1→L	0.64688	3.1371	0.0916	395.22	ILCT/MLCT
		H-2→L	-0.23086				ILCT/MLCT
	3	H-1→L	0.20773	3.2577	0.0151	380.59	ILCT/MLCT
		H-2→L	0.64985				ILCT/MLCT
	4	H-4→L	-0.18273	3.6098	0.0090	343.46	ILCT
		H→L+2	0.65655				LMCT/ILCT

Bar graph 1 exhibits the graphical representation of the electronic absorption parameters corresponding to the lowest energy absorption in all the complexes (λ is taken in μm for simplicity in plotting).

It is seen from Table 3 that the HOMOs of all the complexes are primarily based on the coordinated benzaldimine ligand with a substantial contribution from the ruthenium center. The LUMOs, on the other hand, are localized almost entirely on the bonded benzaldimine moiety and are concentrated largely on the imine fragment. The absorption spectra of all the complexes in the vacuum show four prominent bands. The lowest energy absorption in the range of 688-720 nm is attributed to a HOMO→LUMO transition, and based on the compositions of the orbitals taking part- the excitation is assigned mostly to an intra-ligand charge transfer (ILCT) transition, with a considerable metal-to-ligand charge transfer (MLCT) character. The next two lower energy absorptions have significant involvement of HOMO-1→LUMO, HOMO-2→LUMO, and HOMO-3→LUMO transitions. The highest energy absorption spanning between 343 to 349 nm is a combination of many transitions with an important contribution from HOMO→LUMO+2 transitions.

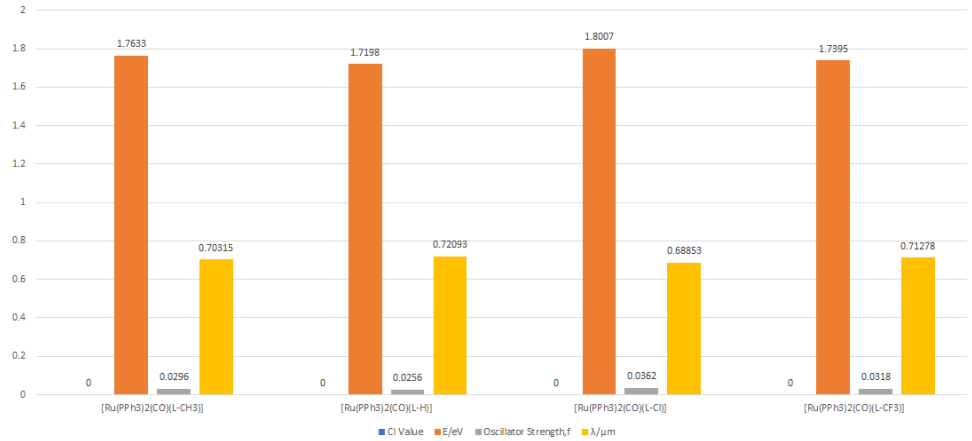

Bar graph 1. Graphical representation of the absorption spectral data corresponding to the lowest energy absorption of the four complexes.

Table 5 records the spectral data of the complexes in a vacuum and three different solvents. The corresponding spectra of the complexes are presented in Fig. 4. In each complex, the lowest energy absorption wavelength decreases consistently with the increase in the polarity of the solvent. This blue shift with an increase in polarity shows that the ground state of the complexes is more polar than the excited states. This can be corroborated by the fact that since the composition of HOMO has a sufficient contribution from the ruthenium center, the d electrons of the metal are transferred to the vacant π^*-orbital of the imine fragment, which remains localized mainly on LUMO. This electronic transition decreases the polarity of the excited state. As a result, the excited state is less stabilized by polar solvents compared to the ground state. So, the lowest energy absorptions have an adequate MLCT contribution to cause a slight blue shift as the polarity of the solvent increases.

Table 5. Absorption wavelengths [nm] and corresponding intensities of the complexes in a vacuum and in different solvents.

Complexes	Vacuum	DCM	Ethanol	DMSO
$[Ru(PPh_3)_2(CO)(L\text{-}CH_3)]$	703.15 (0.0296)	676.72 (0.0391)	672.80 (0.0353)	668.45 (0.0386)
	387.11 (0.1034)	386.95 (0.1410)	386.38 (0.0969)	386.17 (0.1370)
	372.67 (0.0027)	367.61 (0.0348)	367.49 (0.0037)	364.82 (0.0402)
	349.43 (0.0123)	332.68 (0.0270)	346.34 (0.0207)	329.85 (0.0285)
$[Ru(PPh_3)_2(CO)(L\text{-}H)]$	720.93 (0.0256)	694.38 (0.0338)	689.43 (0.0383)	685.70 (0.0333)
	390.41 (0.0962)	389.60 (0.1325)	388.65 (0.1250)	388.72 (0.1275)
	379.31 (0.0128)	372.73 (0.0347)	366.53 (0.0249)	370.03 (0.0400)
	344.78 (0.0070)	329.32 (0.0445)	335.93 (0.1018)	328.79 (0.0915)
$[Ru(PPh_3)_2(CO)(L\text{-}Cl)]$	688.53 (0.0362)	668.79 (0.0475)	662.76 (0.0454)	661.43 (0.0469)
	389.11 (0.1011)	389.28 (0.1397)	388.44 (0.1300)	388.62 (0.1342)
	375.59 (0.0075)	371.24 (0.0266)	369.48 (0.0299)	369.06 (0.0323)
	344.57 (0.0269)	339.06 (0.0684)	338.61 (0.0774)	338.42 (0.0847)
$[Ru(PPh_3)_2(CO)(L\text{-}CF_3)]$	712.78 (0.0318)	691.90 (0.0414)	685.54 (0.0396)	684.09 (0.0408)
	395.22 (0.0916)	394.90 (0.1314)	394.02 (0.1231)	394.22 (0.1269)
	380.59 (0.0151)	377.95 (0.0290)	376.22 (0.0316)	375.81 (0.0340)
	343.46 (0.0090)	339.77 (0.0408)	343.13 (0.0696)	337.88 (0.0281)

3.4. *Natural bond orbital analysis*

To investigate the nature of bonding and electron distribution between the metal center and the coordinating sites of the ligand, an NBO calculation was performed. The calculated charge distribution of the complexes and the corresponding ligands are shown in Table 6. It shows that the electron density of the metal center has increased, the formal charge being changed from +2 before complexation to around -0.8 in the complexes. Such negative values of formal charge on ruthenium, in its complexes, are well documented in the literature [66-68]. The total electron counts of the ruthenium center, shown in Table 7, agree with the negative formal charge on the metal in the complexes. Again, the electron densities of the donor atoms show a reduction in the complexes from those in the free ligand suggesting the transfer of electron density from these atoms to the metal center. In addition, the electron density on ruthenium decreases in the order $[Ru(PPh_3)_2(CO)(L\text{-}$

CH_3)]>[Ru(PPh_3)$_2$(CO)(L-H)]>[Ru(PPh_3)$_2$(CO)(L-Cl)]>[Ru(PPh_3)$_2$(CO)(L-CF_3)] (Table 7). The trend reveals that H_2L-CH_3 has the most donating ability and H_2L-CF_3 the least, as is expected from the inductive effect of the *para*-substituents. The transfer of electron density, on complexation, from the ligand to the metal center can also be understood by studying the occupancy of the associated bonds. The electron density of the relevant bonds of [Ru(PPh_3)$_2$(CO)(L-H)] and the corresponding ligand (H_2L-H) are given in Table 8, and those of the other three complexes and ligands are shown in Table S3 (Supporting Information). The C12-O2 bond has an electron density of 1.99406 in the free ligand, which gets reduced to 1.98654 on bonding (C83-O4). Similar effects are observed for the bonds connected to the other coordinating atoms. Table 8 also lists the hybridization of ruthenium and the donor atoms, the % contribution of the bonding atoms and atomic orbitals (AO) to the bonds. It is found that ruthenium generally exists in an sp^3d^2 hybridized state, with variations depending on the particular bond demonstrating that the complexes are distorted octahedral, as is also evident from the bond parameters.

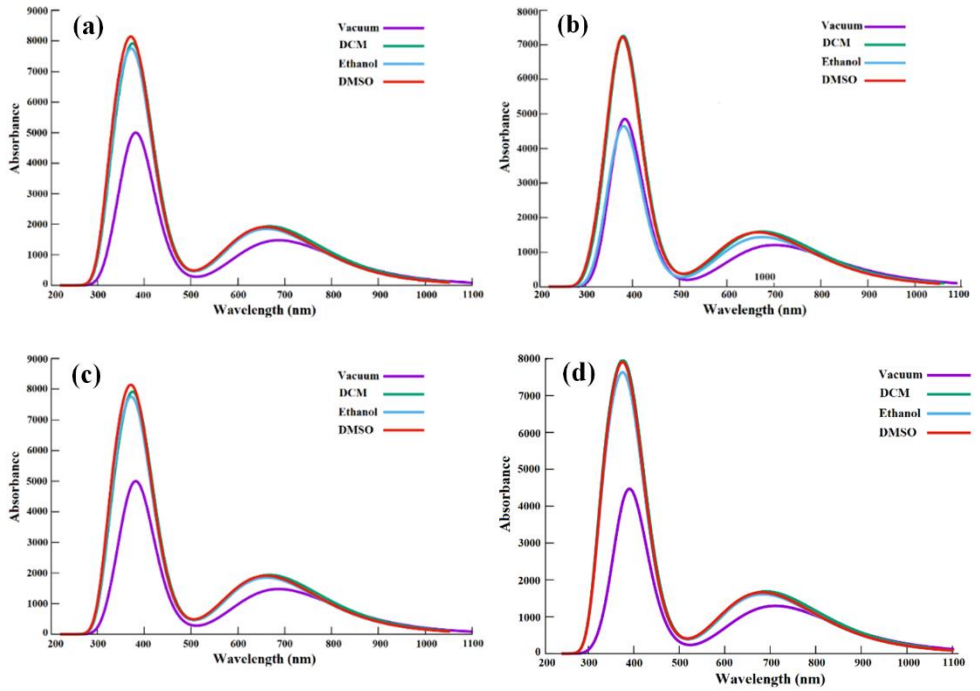

Fig. 4. UV-Vis spectra of a) [Ru(PPh_3)$_2$(CO)(L-CH_3)] b) [Ru(PPh_3)$_2$(CO)(L-H)] c) [Ru(PPh_3)$_2$(CO)(L-Cl)] d) [Ru(PPh_3)$_2$(CO)(L-CF_3)] in vacuum and three different solvents.

Table 6. Natural charges [a.u] on ruthenium and donor atoms in the complexes and corresponding ligands.

Complexes and corresponding free ligands	Atoms						
	Ru	N	O	C (orthometallated in complexes)	P5	P6	C (CO)
$[Ru(PPh_3)_2(CO)(L\text{-}CH_3)]$	-0.83770	-0.34417	-0.65693	-0.00374	1.15585	1.19154	0.68310
$H_2L\text{-}CH_3$	-	-0.48018	-0.70401	-0.17840	-	-	-
$[Ru(PPh_3)_2(CO)(L\text{-}H)]$	-0.83712	-0.33733	-0.65605	-0.01456	1.15599	1.19153	0.68348
$H_2L\text{-}H$	-	-0.47545	-0.70355	-0.18993	-	-	-
$[Ru(PPh_3)_2(CO)(L\text{-}Cl)]$	-0.83362	-0.33690	-0.65349	-0.00742	1.15625	1.19166	0.68567
$H_2L\text{-}Cl$	-	-0.47207	-0.67949	-0.18618	-	-	-
$[Ru(PPh_3)_2(CO)(L\text{-}CF_3)]$	-0.81923	-0.33254	-0.66032	-0.00958	1.24485	1.28333	0.74452
$H_2L\text{-}CF_3$	-	-0.46556	-0.70106	-0.20265	-	-	-

Table 7. Allotment of ruthenium electrons between core, valence, and Rydberg orbitals.

Complexes	Core	Valence	Rydberg	Total
$[Ru(PPh_3)_2(CO)(L\text{-}CH_3)]$	35.97360	8.82030	0.04380	44.83770
$[Ru(PPh_3)_2(CO)(L\text{-}H)]$	35.97363	8.82033	0.04317	44.83713
$[Ru(PPh_3)_2(CO)(L\text{-}Cl)]$	35.97361	8.81683	0.04318	44.83362
$[Ru(PPh_3)_2(CO)(L\text{-}CF_3)]$	35.97307	8.80196	0.04420	44.81923

Table 8. Natural bond orbital analysis of selected bonds in $[Ru(PPh_3)_2(CO)(L\text{-}H)]$ and $H_2L\text{-}H$.

Bond	Occupancy	% contribution	Hybridization	AO %
$[Ru(PPh_3)_2(CO)(L\text{-}H)]$				
Ru1-N2	1.89815	Ru-18.01, N-81.99	Ru-sp4.22d3.73, N-sp1.49	Ru-s(11.17) p(47.18) d(41.65) N-s(40.12) p(59.88)
Ru1-P5	1.81267	Ru-28.70, P-71.30	Ru-sp2.78d1.75, P-sp2.33	Ru-s(18.07) p (50.22) d(31.71) P-s(30.01) p(69.99)
Ru1-P6	1.78800	Ru-30.27, P-69.73	Ru-sp3.12d2.13, P-sp2.32	Ru-s(15.99) p(49.92) d(34.08) P-s(30.10)p(69.90)
Ru1-C73	1.87730	Ru-31.42, C-68.58	Ru-sp2.93d1.72, C-sp0.48	Ru-s(17.69) p(51.90) d(30.41) C-s(67.51) p(32.49)
Ru1-C95	1.85475	Ru-37.17, C-62.83	Ru-sp0.56d2.09, C- sp2.18	Ru-s(27.42) p(15.30) d(57.28) C-s(31.43) p(68.57)
N2-C74	1.97671	N-60.89, C-39.11	N-sp2.81 C-sp2.66	N-s(26.24) p(73.76) C-s(27.33) p(72.67)
N2-C84 (σ)	1.98134	N-61.11 C-38.89	N-sp1.98 C-sp2.45	N-s(27.33) p(72.67) C-s(29.00) p(71.00)
N2-C84 (π)	1.91350	N-61.09 C-38.91	N-sp99.99 C-sp99.99	N-s(0.19) p(99.81) C-s(0.01) p(99.99)
O4-C83	1.98654	O-63.75 C-36.25	O-sp2.27 C-sp2.65	O-s(30.62) p(69.38) C-s(27.38) p(72.62)
$H_2L\text{-}H$ (Fig. S1)				
N1-C3	1.98287	N-58.68, C-41.32	N-sp2.52 C-sp2.72	N-s(28.40) p(71.60) C-s(26.86) p(73.14)

N1-C13	1.98718	N-59.40	N-sp1.79	N-s(35.79) p(64.21)
(σ)		C-40.60	C-sp2.50	C-s(28.61) p(71.39)
N1-C13	1.90209	N-58.13	N-sp99.99	N-s(0.02) p(99.98)
(π)		C-41.87	C-sp99.99	C-s(0.02) p(99.98)
O2-C12	1.99406	O-66.38	O-sp1.82	O-s(35.46) p(64.54)
		C-33.62	C-sp2.98	C-s(25.12) p(74.88)

4. Conclusion

The current work investigates the structural and electronic properties of a group of ruthenium-Schiff base complexes with the help of density functional theory. The optimized geometry of $[Ru(PPh_3)_2(CO)(L\text{-}H)]$ in the ground state reveals that the geometrical parameters conform well to the experimental values. The energies of HOMO and LUMO of the complexes along with global indices, *viz*., chemical potential, chemical hardness, and electrophilicity index are calculated, which show the reactivity order of the complexes to be $[Ru(PPh_3)_2(CO)(L\text{-}CF_3)]$>$[Ru(PPh_3)_2(CO)(L\text{-}CH_3)]$>$[Ru(PPh_3)_2(CO)(L\text{-}H)]$>$[Ru\ (PPh_3)_2(CO)(L\text{-}Cl)]$. The electronic spectra of the complexes, as interpreted by TDDFT calculations, exhibit that the lowest energy absorptions are HOMO→LUMO transitions and are predominantly ILCT in character with a prominent MLCT contribution. These lowest energy absorptions display a blue shift with the increase in polarity of the solvent in all the complexes. The NBO calculations are in accordance with a significant shift in electron density from the coordinating atoms to the metal center. The hybridizations of ruthenium and the donor atoms, the atomic orbital (AO) % to the metal-donor bonds, are all in good accordance with the structure of the complexes.

Acknowledgments

The author thanks S. Giri, School of Applied Sciences and Humanities, Haldia Institute of Technology, for his help with Gaussian 16 software and its calculations. The author expresses deep gratitude and thankfulness to R. T. Dey, Department of Chemistry, Government General Degree College, Muragachha, who helped with his constructive comments in preparing the manuscript. The author thanks the Department of Chemistry, Hooghly Mohsin College, Chinsurah, Hooghly.

References

1. R. B. Moffett and N. Rabjohn Edited, Organic Syntheses (John Wiley & Sons, Inc.: New York, USA, 1963) **4**, pp. 605–608.
2. A. S. Shekhawat, N. P. Singh, and N. S. Chundawat, J. Sci. Res. **14**, 387 (2022). https://doi.org/10.3329/jsr.v14i1.54814
3. R. Kalarani, M. Sankarganesh, G. G. V. Kumar, and M. Kalanithi, J. Mol. Str. **1206**, ID 127725 (2020). https://doi.org/10.1016/j.molstruc.2020.127725
4. A. B. Deilami, M. Salehi, A. Amiri, and A. Arab, J. Mol. Str. **1181**, 190 (2019). https://doi.org/10.1016/j.molstruc.2018.12.031

5. K. Andiappan, A. Sanmugam, E. Deivanayagam, K. Karuppasamy, H. -S. Kim, and D. Vikraman, Int. J. Biol. Macromol. **124**, 403 (2019). https://doi.org/10.1016/j.ijbiomac.2018.11.251
6. O. M. I. Adly, H. F. El-Shafiy, and M. Shebl, J. Mol. Str. **1196**, 805 (2019). https://doi.org/10.1016/j.molstruc.2019.07.010
7. X. Liu and J. -R. Hamon, Coord. Chem. Rev. **389**, 94 (2019). https://doi.org/10.1016/j.ccr.2019.03.010
8. A. B. Deilami, M. Salehi, A. Arab, and A. Amiri, Inorg. Chim. Acta **476**, 93 (2018). https://doi.org/10.1016/j.ica.2018.02.013
9. F. Sevgi, U. Bagkesici, A. N. Kursunlu, and E. Guler, J. Mol. Str. **1154**, 256 (2018). https://doi.org/10.1016/j.molstruc.2017.10.052
10. I. Rajaei and S. N. Mirsattari, J. Mol. Str. **1163**, 236 (2018). https://doi.org/10.1016/j.molstruc.2018.02.010
11. J. Tang, H. -Y. Yin, and J. -L. Zhang, Chem. Sci. **9**, 1931 (2018). https://doi.org/10.1039/C7SC04498D
12. J. Zhang, L. Xu, and W. -Y. Wong, Coord. Chem. Rev. **355**, 180 (2018). https://doi.org/10.1016/j.ccr.2017.08.007
13. K. R. Balinge, A. G. Khiratkar, and P. R. R. Bhagat, J. Organomet. Chem. **854**, 131 (2018). https://doi.org/10.1016/j.jorganchem.2017.11.022
14. M. T. Kaczmarek, M. Zabiszak, M. Nowak, and R. Jastrzab, Coord. Chem. Rev. **370**, 42 (2018). https://doi.org/10.1016/j.ccr.2018.05.012
15. S. Mondal, M. Chakraborty, A. Mondal, B. Pakhira, A. J. Blake, E. Sinn, and S. K. Chattopadhyay, New J. Chem. **42**, 9588 (2018). https://doi.org/10.1039/C8NJ00418H
16. A. C. Ekennia, A. A. Osowole, L. O. Olasunkanmi, D. C. Onwudiwe, O. O. Olubiyi, and E. E. Ebenso, J. Mol. Str. **1150**, 279 (2017). https://doi.org/10.1016/j.molstruc.2017.08.085
17. R. Fekri, M. Salehi, A. Asadi, and M. Kubicki, Polyhedron **128**, 175 (2017). https://doi.org/10.1016/j.poly.2017.02.047
18. Sh. M. Morgan, A. Z. El-Sonbati, and H. R. Eissa, J. Mol. Liq. **240**, 752 (2017). https://doi.org/10.1016/j.molliq.2017.05.114
19. P. Das and W. Linert, Coord. Chem. Rev. **311**, 1 (2016). https://doi.org/10.1016/j.ccr.2015.11.010
20. Q. -M. Hasi, Y. Fan, X. -Q. Yao, D. -C. Hu, and J. -C. Liu, Polyhedron **109**, 75 (2016). https://doi.org/10.1016/j.poly.2016.01.052
21. W. A. Zoubi and Y. G. Ko, J. Organomet. Chem. **822**, (2016), 173. https://doi.org/10.1016/j.jorganchem.2016.08.023
22. Z. Li, H. Yan, G. Chang, M. Hong, J. Dou, and M. Niu, J. Photochem. Photobiol. B **163**, 403 (2016). https://doi.org/10.1016/j.jphotobiol.2016.09.005
23. M. Hajrezaie, M. Paydar, C. Y, Looi, S. Z. Moghadamtousi, P. Hassandarvish, K. Salga, H. Karimian, K. Shams, M. Zahedifard, N. A. Majid, H. M. Ali, and M. A. Abdulla, Sci. Rep. **5**, 9097 (2015). https://doi.org/10.1038/srep09097
24. Y. Jia and J. Li, Chem. Rev. **115**, 1597 (2015). https://doi.org/10.1021/cr400559g
25. H. P. Ebrahimi, J. S. Hadi, and Z. A. Abdulnabi, and Z. Bolandnazar, Spectrochim. Acta Part A **117**, 485 (2014). https://doi.org/10.1016/j.saa.2013.08.044
26. C. -G. Liu, Y. -Q. Qiu, S. -L. Sun, N. Li, G. -C. Yang, and Z. -M. Su, Chem. Phys. Lett. **443**, 163 (2007). https://doi.org/10.1016/j.cplett.2007.06.060
27. C. G. Roy, S. S. Sen, S. Dutta, G. Mostafa, and S. Bhattacharya, Polyhedron **26**, 3876 (2007). https://doi.org/10.1016/j.poly.2007.04.020
28. H. A. Hassanin and A. A. Abdel-Shafi, J. Photochem. Photobiol. A **424**, ID 113635 (2022). https://doi.org/10.1016/j.jphotochem.2021.113635.
29. R. Gramage-Doria and C. Bruneau, Coord. Chem. Rev. **428**, ID 213602 (2021). https://doi.org/10.1016/j.ccr.2020.213602
30. D. Havrylyuk, D. K. Heidary, Y. Sun, S. Parkin, and E. C. Glazer, ACS Omega **5**, 18894 (2020). https://doi.org/10.1021/acsomega.0c02079

31. D. M. Yufanyi, H. S. Abbo, S. J. J. Titinchi, and T. Neville, Coord. Chem. Rev. **414**, ID 213285 (2020). http://doi.org/10.1016/j.ccr.2020.213285
32. S-C. Chan and C-Y. Wong, Coord. Chem. Rev. **402**, ID 213082 (2020). https://doi.org/10.1016/j.ccr.2019.213082
33. A. Jain, Coord. Chem. Rev. **401**, ID 213067 (2019). https://doi.org/10.1016/j.ccr.2019.213067
34. A. R. Simović, R. Masnikosa, I. Bratsos, and E. Alessio, Coord. Chem. Rev. **398**, 113011 (2019). http://dx.doi.org/10.1016/j.ccr.2019.07.008
35. F. D. Abreu, T. de F. Paulo, M. H. Gehlen, R. A. Ando, L. G. F. Lopes, A. C. S. Gondim, M. A. Vasconcelos, E. H. Teixeira, E. H. S. Sousa, and I. M. M. de Carvalho, Inorg. Chem. **56**, 9084 (2017). https://doi.org/10.1021/acs.inorgchem.7b01108
36. Q. Sun, S. Mosquera-Vazquez, Y. Suffren, J. Hankache, N. Amstutz, L. Max, L. Daku, E. Vauthey, and A. Hauser, Coord. Chem. Rev. **282-283**, 87 (2015). https://doi.org/10.1016/j.ccr.2014.07.004
37. G. C. Vougioukalakis and R. H. Grubbs, Chem. Rev. **110**, 1746 (2010). https://doi.org/10.1021/cr9002424
38. L-Q. Chai, X-F. Zhang, and L-J. Tang, J. Mol. Str. **1245**, ID 131028 (2021). https://doi.org/10.1016/j.molstruc.2021.131028
39. K. P. Kepp, Coord. Chem. Rev. **257**, 196 (2013). https://doi.org/10.1016/j.ccr.2012.04.020
40. S. J. Konezny, M. D. Doherty, O. R. Luca, R. H. Crabtree, G. L. Soloveichik, and V. S. Batista, J. Phys. Chem. C **116**, 6349 (2012). http://doi.org/10.1021/jp300485t
41. T. F. Hughes and R. A. Friesner, J. Chem. Theory Comput. **8**, 442 (2012). https://doi.org/10.1021/ct2006693
42. F. Neese, Coord. Chem. Rev. **253**, 526 (2009). https://doi.org/10.1016/j.ccr.2008.05.014
43. F. Rastrelli and A. Bagno, Chem.-Eur. J. **15**, 7990 (2009). https://doi.org/10.1002/chem.200802443
44. L. Salassa, C. Garino, G. Salassa, R. Gobetto, and C. Nervi, J. Am. Chem. Soc. **130**, 9590 (2008). https://doi.org/10.1021/ja8025906
45. S. Yadav, A. Khare, K. K. Yadav, P. C. Maurya, A. K. Singh, and A. Kumar, J. Sci. Res. **14**, 79 (2022). https://doi.org/10.3329/jsr.v14i1.53339
46. H. Yu, Y. Fu, Q. Guo, and Z. Lin, Organometallics **28**, 4443 (2009). https://doi.org/10.1021/om9002957
47. D. Cho, K. C. Ko, and J. Y. Lee, Organometallics **32**, 4571 (2013). https://doi.org/10.1021/om4005324
48. F. Bernardi, A. Bottoni, and G. P. Miscione, Organometallics **22**, 940 (2003). https://doi.org/10.1021/om020536o
49. M. J. Frisch et al., Gaussian 16, Revision C.01 (Gaussian, Inc., Wallingford CT, 2016).
50. L. W. Chung, W. M. C. Sameera, R. Ramozzi, A. J. Page, M. Hatanaka, G. P. Petrova, T. V. Harris, X. Li, Z. Ke, F. Liu, H-B. Li, L. Ding, and K. Morokuma, Chem. Rev. **115**, 5678 (2015). https://doi.org/10.1021/cr5004419
51. L. Li, J. Hu, X. Shi, W. Ruan, J. Luo, and X. Wei, Int. J. Mol. Sci. **17**, 927 (2016). http://doi.org/10.3390/ijms17060927
52. T. Österman and P. Persson, Chem. Phy. **407**, 76 (2012). https://doi.org/10.1016/j.chemphys.2012.09.001
53. S. L. -F. Chan, Y. -H. Kan, K. -L. Yip, J. -S. Huang, and C. -M. Che, Coord. Chem. Rev. **255**, 899 (2011). https://doi.org/10.1016/j.ccr.2010.11.026
54. X. Lu, S. Wei, C. -M. L. Wu, W. Guo, and L. Zhao, J. Org. Chem. **696**, 1632 (2011). https://doi.org/10.1016/j.jorganchem.2011.01.030
55. J. Dutta, M. G. Richmond, and S. Bhattacharya, Dalton Trans. **44**, 13615 (2015). https://doi.org/10.1039/C5DT01564B
56. S. Pratihar and S. Roy, J. Org. Chem. **75**, 4957 (2010). https://doi.org/10.1021/jo100425a
57. R. G. Pearson, J. Chem. Sci. **117**, 369 (2005). https://doi.org/10.1007/BF02708340
58. G. O. Tarı, Ü. Ceylan, E. Agar, and H. Eserci, J. Mol. Str. **1126**, 83 (2016). http://doi.org/10.1016/JMOLSTRUC.2016.01.058

59. A. Zülfikaroglu, H. Batı, and N. Dege, J. Mol. Str. **1162**, 125 (2018). https://doi.org/10.1016/j.molstruc.2019.02.109
60. K. Fukui, T. Yonezawa, C. Nagata, and H. Shingu, J. Chem. Phys. **22**, 1433 (1954). https://doi.org/10.1063/1.1740412
61. K. Fukui, T. Yonezawa, and H. Shingu, J. Chem. Phys. **20**, 722 (1952). https://doi.org/10.1063/1.1700523
62. S. AlAbbad, T. Sardot, O. Lekashvili, D. Decato, F. Lelj, J. B. A. Ross, and E. Rosenberg, J. Mol. Str. **1195**, 620 (2019). https://doi.org/10.1016/j.molstruc.2019.06.005
63. M. Yoosefian and N. Etminan, RSC Adv. **6**, 64818 (2016). https://doi.org/10.1039/C6RA14006H
64. R. Ghiasi and M. M. Mehrabani, J. Theo. Comp. Chem. **12**, 1350071 (2013). https://doi.org/10.1142/S0219633613500715
65. X. -J. Liu, J. -K. Feng, J. Meng, Q. -J. Pan, A. -M. Ren, X. Zhou, and H. -X. Zhang, Eur. J. Inorg. Chem. 1856 (2005). https://doi.org/10.1002/ejic.200400533
66. F. Hayat, Zia-ur-Rehman, and M. H. Khan, J. Coord. Chem. **70**, 279 (2017). https://doi.org/10.1080/00958972.2016.1255328
67. S. Biswas, P. Roy, D. Sarkar, and T. K. Mondal, Indian J. Chem. **55A**, 929 (2016).
68. W. Sharmoukh, W. M. I. Hassan, P. C. Gros, and N. K. Allam, RSC Adv. **6**, 69647 (2016). https://doi.org/10.1039/C6RA16458G

Supporting information

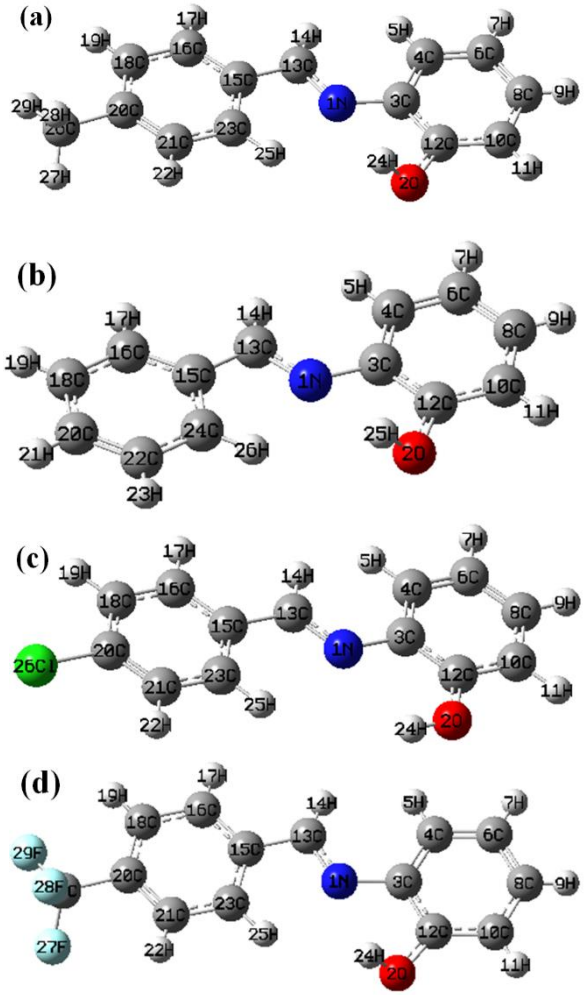

Fig. S1. Optimized structure of a) H_2L-CH_3 b) H_2L-H c) H_2L-Cl d) H_2L-CF_3.

Table S1. Optimized bond distances (Å) and bond angles (°) of $[Ru(PPh_3)_2(CO)(L\text{-}CH_3)]$, $[Ru(PPh_3)_2(CO)(L\text{-}Cl)]$ and $[Ru(PPh_3)_2(CO)(L\text{-}CF_3)]$.

$[Ru(PPh_3)_2(CO)(L\text{-}CH_3)]$			
Bond Distances (Å)			
Ru1-P5	2.41901	Ru1-N2	2.11587
Ru1-P6	2.42694	Ru1-C94	2.07235
Ru1-O4	2.21023	Ru1-C73	1.85020
Bond Angles (°)			
P6-Ru1-P5	177.219	C94-Ru1-N2	79.628
C94-Ru1-O4	156.564	N2-Ru1-O4	76.940
C73-Ru1-N2	175.995	Ru1-C73-O3	177.277
$[Ru(PPh_3)_2(CO)(L\text{-}Cl)]$			
Bond Distances (Å)			
Ru1-P5	2.37081	Ru1-N2	2.11780
Ru1-P6	2.37574	Ru1-C94	2.07514
Ru1-O4	2.21063	Ru1-C73	1.86175
Bond Angles (°)			
P6-Ru1-P5	175.978	C94-Ru1-N2	79.353
C94-Ru1-O4	156.014	N2-Ru1-O4	76.669
C73-Ru1-N2	176.332	C73-Ru1-N2	177.695
$[Ru(PPh_3)_2(CO)(L\text{-}CF_3)]$			
Bond Distances (Å)			
Ru1-P5	2.37152	Ru1-N2	2.11783
Ru1-P6	2.37468	Ru1-C94	2.07560
Ru1-O4	2.21172	Ru1-C73	1.86190
Bond Angles (°)			
P6-Ru1-P5	175.984	C94-Ru1-N2	79.302
C94-Ru1-O4	155.947	N2-Ru1-O4	76.668
C73-Ru1-N2	176.457	C73-Ru1-N2	176.457

Table S2**.** Composition of molecular orbitals associated with electronic absorption of the complexes.

Complexes	Molecular Orbitals	Contribution of Fragments (%)			
		Ru	L-R	CO	PPh_3
$[Ru(PPh_3)_2(CO)(L\text{-}CH_3)]$	L+2	53	9	11	27
	L+1	34	22	32	12
	H-1	57	30	11	2
	H-2	44	46	2	8
	H-3	37	56	4	3
$[Ru(PPh_3)_2(CO)(L\text{-}H)]$	L+2	59	6	12	23
	L+1	39	14	37	10
	H-1	56	30	12	2
	H-2	42	51	1	6
	H-3	38	55	5	2
$[Ru(PPh_3)_2(CO)(L\text{-}Cl)]$	L+2	62	6	14	18
	L+1	41	20	22	17
	H-1	56	30	12	2
	H-2	42	46	2	10
	H-3	33	60	4	3
	H-4	11	51	0	38
$[Ru(PPh_3)_2(CO)(L\text{-}CF_3)]$	L+2	62	8	11	19

	L+1	39	23	21	17
	H-1	57	30	12	1
	H-2	40	48	1	11
	H-3	41	50	5	4
	H-4	6	51	1	42

Table S3. Natural bond orbital analysis of selected bonds in the complexes and corresponding ligands.

Bond	Occupancy	% Contribution	Hybridization	AO %
$[Ru(PPh_3)_2(CO)(L\text{-}CH_3)]$				
Ru1-N2	1.89734	Ru-18.62, N-81.38	Ru-$sp^{3.12}d^{3.88}$, N-$sp^{2.30}$	Ru-s(14.00) p(51.76) d(34.24) N-s(32.22) p(67.78)
Ru1-P5	1.81785	Ru-29.05, P-70.95	Ru-$sp^{3.33}d^{2.20}$, P-$sp^{2.33}$	Ru-s(15.31) p(50.98) d(33.71) P-s(30.04) p(69.96)
Ru1-P6	1.79694	Ru-30.87, P-69.13	Ru-$sp^{4.04}d^{3.00}$, P-$sp^{2.32}$	Ru-s(12.44) p(50.24) d(37.32) P-s(30.13) p(69.17)
Ru1-C73	1.93627	Ru-35.11, C-64.89	Ru-$sp^{0.79}d^{1.70}$, C-$sp^{0.48}$	Ru-s(28.68) p(22.62) d(48.71) C-s(67.51) p(32.49)
Ru-C94	1.88512	Ru-38.94, C-61.06	Ru-$sp^{0.67}d^{3.42}$, C- $sp^{2.19}$	Ru-s(19.68) p(13.12) d(67.20) C-s(31.34) p(68.66)
N2-C74	1.96852	N-61.18, C-38.82	N-$sp^{2.97}$ C-$sp^{2.53}$	N-s(25.16) p(74.84) C-s(28.31) p(71.69)
N2-C84 (σ)	1.97979	N-61.09 C8-38.91	N-$sp^{1.74}$ C-$sp^{2.45}$	N-s(36.45) p(63.55) C-s(29.02) p(70.98)
N2-C84 (π)	1.91354	N-74.46 C-25.54	N-$sp^{99.99}$ C-$sp^{99.99}$	N-s(0.35) p(99.65) C-s(0.01) p(99.99)
O4-C83	1.98653	O-63.76 C-36.24	O-$sp^{2.26}$ C-$sp^{2.65}$	O-s(30.64) p(69.36) C-s(23.84) p(76.16)
$H_2L\text{-}CH_3$				
N1-C3	1.98283	N-58.65, C-41.35	N-$sp^{2.52}$ C-$sp^{2.72}$	N-s(28.39) p(71.61) C-s(26.88) p(73.12)
N1-C13 (σ)	1.98716	N-59.38 C-40.62	N-$sp^{1.79}$ C-$sp^{2.49}$	N-s(35.80) p(64.20) C-s(28.62) p(71.38)
N1-C13 (π)	1.90289	N-58.35 C-41.65	N-$sp^{99.99}$ C-$sp^{99.99}$	N-s(0.02) p(99.98) C-s(0.02) p(99.98)
O2-C12	1.99406	O-66.39 C-33.61	O-$sp^{1.82}$ C-$sp^{2.98}$	O-s(35.48) p(64.52) C-s(25.12) p(74.88)
$[Ru(PPh_3)_2(CO)(L\text{-}Cl)]$				
Ru1-N2	1.90013	Ru-18.44, N-81.56	Ru-$sp^{4.13}d^{2.89}$, N-$sp^{2.25}$	Ru-s(13.52) p(49.22) d(37.26) N-s(38.76) p(61.24)
Ru1-P5	1.81634	Ru-29.23, P-70.77	Ru-$sp^{3.32}d^{2.20}$, P-$sp^{2.35}$	Ru- s(15.34) p(50.97) d(33.69) P- s(29.88) p(70.12)
Ru1-P6	1.79516	Ru-31.05, P-69.13	Ru-$sp^{4.03}d^{2.99}$, P-$sp^{2.34}$	Ru-s(12.45) p(50.25) d(37.29) P-s(29.97) p(70.03)
Ru1-C73	1.93633	Ru-35.13, C-64.87	Ru-$sp^{0.79}d^{1.70}$, C-$sp^{0.48}$	Ru-s(28.71) p(22.54) d(48.75) C-s(67.46) p(32.54)
Ru1-C94	1.88408	Ru-38.30, C-61.70	Ru-$sp^{0.67}d^{3.41}$, C- $sp^{2.14}$	Ru-s(19.68) p(13.22) d(67.10) C-s(31.90) p(68.10)
N2-C74	1.96852	N-61.27, C-38.73	N-$sp^{2.97}$ C-$sp^{2.53}$	N-s(25.22) p(74.78) C-s(28.30) p(71.70)
N2-C84	1.97978	N-61.08	N-$sp^{1.75}$	N-s(36.40) p(63.60)

(σ)		C-38.92	C-$sp^{2.44}$	C-s(29.04) p(70.96)
N2-C84	1.91185	N-60.85	N-sp^{100}	N-s(0.00) p(100.00)
(π)		C-39.15	C-$sp^{99.99}$	C-s(0.01) p(99.99)
O4-C83	1.98646	O-63.78	O-$sp^{2.27}$	O-s(30.60) p(69.40)
		C-36.22	C-$sp^{2.65}$	C-s(27.36) p(72.64)
H_2L-Cl				
N1-C3	1.98019	N-59.02	N-$sp^{2.26}$	N-s(30.67) p(69.33)
		C-40.9	C-$sp^{2.84}$	C-s(26.01) p(73.99)
N1-C13	1.99011	N-59.87	N-$sp^{1.61}$	N-s(38.33) p(61.67)
(σ)		C-40.13	C-$sp^{2.17}$	C-s(31.57) p(68.43)
N1-C13	1.92004	N-57.33	N-sp^{100}	N-s(0.00) p(100.00)
(π)		C-42.67	C-sp^{100}	C-s(0.00) p(100.00)
O2-C12	1.99007	O-66.88	O-$sp^{1.43}$	O-s(41.13) p(58.87)
		C-33.12	C-$sp^{2.94}$	C-s(25.40) p(74.60)
$[Ru(PPh_3)_2(CO)(L\text{-}CF_3)]$				
Ru1-N2	1.89671	Ru-18.16,	Ru-$sp^{4.36}d^{3.85}$,	Ru-s(10.86) p(47.37) d(41.78)
		N-81.84	N-$sp^{1.53}$	N-s(39.58) p(60.42)
Ru1-P5	1.79940	Ru-30.27,	Ru-$sp^{2.74}d^{1.72}$,	Ru-s(18.32) p (50.13) d(31.55)
		P-69.73	P-$sp^{2.41}$	P-s(29.30) p(70.58) d (0.12)
Ru1-P6	1.77281	Ru-31.97,	Ru-$sp^{3.09}d^{2.08}$,	Ru-s(16.22) p(50.07) d(33.71)
		P-68.03	P-$sp^{2.39}$	P-s(29.42) p(70.44) d(0.14)
Ru1-C73	1.87304	Ru-31.94,	Ru-$sp^{2.95}d^{1.75}$,	Ru-s(17.53) p(51.72) d(30.75)
		C-68.06	C-$sp^{0.49}$	C-s(66.96) p(33.04)
Ru1-C94	1.85361	Ru-36.99,	Ru-$sp^{0.59}d^{2.13}$,	Ru-s(26.87) p(15.86) d(57.26)
		C-63.01	C- $sp^{2.17}$	C-s(31.55) p(68.45)
N2-C74	1.97660	N-61.04,	N-$sp^{2.77}$	N-s(26.54) p(73.41)
		C-38.96	C-$sp^{2.66}$	C-s(29.19) p(70.70)
N2-C84	1.98101	N-61.21	N-$sp^{1.96}$	N-s(33.74) p(66.22)
(σ)		C-38.79	C-$sp^{2.42}$	C-s(29.00) p(71.00)
N2-C84	1.90928	N-60.78	N-$sp^{99.99}d^{0.46}$	N-s(0.19) p(99.73) d(0.09)
(π)		C-39.22	C-$sp^{99.99}$	C-s(0.01) p(99.87)
O4-C83	1.98685	O-64.17	O-$sp^{2.07}$	O-s(32.53) p(67.40)
		C-35.83	C-$sp^{2.65}$	C-s(24.61) p(75.32)
$H_2L\text{-}CF_3$				
N1-C3	1.98297	N-58.86,	N-$sp^{2.50}$	N-s(28.58) p(71.42)
		C-41.14	C-$sp^{2.74}$	C-s(26.76) p(73.24)
N1-C13	1.98720	N-59.42	N-$sp^{1.80}$	N-s(35.71) p(64.29)
(σ)		C-40.58	C-$sp^{2.49}$	C-s(28.62) p(71.38)
N1-C18	1.89962	N-57.52	N-$sp^{99.99}$	N-s(0.02) p(99.98)
(π)		C-42.48	C-$sp^{99.99}$	C-s(0.02) p(99.99)
O2-C12	1.99404	O-66.37	O-$sp^{1.82}$	O-s(35.41) p(64.59)
		C-33.63	C-$sp^{2.98}$	C-s(25.13) p(74.87)